BRAin-wide Neuron quantification Tool reveals strong sexual dimorphism in the evolution of fear memory

Alessandra FRANCESCHINI[1,2]* Giacomo MAZZAMUTO[1,3] Curzio CHECCUCCI[4], Lorenzo CHICCHI[2], Duccio FANELLI[2], Francesco Saverio PAVONE[1,2,3], Ludovico SILVESTRI[1,2,3]*

1 European Laboratory for non-linear Spectroscopy (LENS), University of Florence, Sesto Fiorentino, Italy

2 Department of Physics, University of Florence, Sesto Fiorentino, Italy;

3 *National Institute of Optics - National Research Council (CNR-INO), Sesto Fiorentino, Italy*

4 Department of Information Engineering (DINFO), University of Florence, Florence, Italy

*corresponding authors: franceschini@lens.unifi.it, silvestri@lens.unifi.it

ABSTRACT

The neuronal and molecular mechanisms underlying behavioral responses triggered by fear have received wide interest now, especially with the surge of fear-related disorders associated with the recent Covid-19 pandemic. Fear responses are functionally adaptive behaviors that are strengthened as memories. Indeed, knowing fear circuitry could be the turning point for the comprehension of this emotion and its pathological states, even addressing potential treatments.

Understanding memory dynamics presents fundamental technological challenges and calls for the development of new tools and methods able to analyze the entire brain with single-neuron resolution. In this context, we developed the BRAin-wide Neuron quantification Tool (BRANT) for mapping neuronal activation at micron resolution, combining tissue clearing protocol, high-resolution light-sheet microscopy, and automated 3D image analysis. This method allowed us to quantify the evolution of neuronal activation patterns across multiple phases of memory. This approach highlighted a strong sexual dimorphism in the circuits recruited during memory recall, which had no counterpart in the behaviour. The methodology presented here paves the way for a comprehensive functional characterization of the evolution of fear memory.

INTRODUCTION

Fear responses are functionally adaptive behaviors that are strengthened as memories. Indeed, given its high survival value, the capability to remember potential threats is highly conserved across species (Kindt 2014). Although 'fear' refers to a human emotion, with a specific connotation in our minds that might not be present in other animals, we can nevertheless study the effects of aversive events in animal models using standard behavioral paradigms like contextual fear conditioning (CFC) and inhibitory avoidance (IA) (Izquierdo, Furini, e Myskiw 2016). Fear induces many changes at each brain level, from the molecular and cellular to circuit ones. These permanent changes represent the physical trace of memory, that is commonly referred to as 'engram'. In the last years, neuroscientists have made many steps forward in the knowledge of the molecular and cellular mechanisms underlying memory formation, consolidation and retrieval (Johansen et al. 2011; Tonegawa, Morrissey, e Kitamura 2018; Josselyn e Frankland 2018; Orsini e Maren 2012). Furthermore, several brain areas, most prominently the hippocampus, the amygdala and the prefrontal cortex, have been identified as important centers for memory processing (Izquierdo, Furini, e Myskiw 2016). However, several studies highlighted the involvement of many other regions (Pezzone et al. 1992; Moaddab, Ray, e McDannald 2021; Silva et al. 2021), supporting the hypothesis that memory is distributed and dispersed across the entire brain; in this perspective, the study of a single or few brain areas limits the comprehension of mechanisms underlying fear memory. The study of limited brain regions leads to a fragmented view that makes the global vision rarely interpretable, therefore many significant questions about fear mechanism and dynamics have yet to be explained.

Indeed, the little knowledge of the mechanisms underlying fear memory at brain-wide level is mainly due to the technical limitations in large-scale analysis of neuronal activity. From a methodological point of view, understanding how neuronal networks drive this type of memory requires techniques for whole-brain mapping. Indeed, this technique allows to tag activated neurons *in-vivo* through immediately early gene (IEG) approaches and image them subsequently *ex-vivo* by 3D optical tools such as Light-sheet microscopy (LSM). The coupling of clearing techniques, like CLARITY (Chung et al. 2013), iDISCO (Renier et al. 2014), or CUBIC (Susaki et al. 2014), with LSM has enabled the brain-wide mapping of cFos positive neurons activated during the formation, consolidation and retrieval of fear memory.

From a clinical point of view, the study of fear memory is necessary to clarify how different neuronal circuits are disrupted in disease states as in post-traumatic stress disorder (PTSD). Indeed, understanding how memory works and changes over time could be key for treating PTSD. The lifetime prevalence of this pathology is about 10–12% in women and 5–6% in men (Charak et al. 2014). Women have a two/three times higher risk of developing PTSD compared to men (Christiansen e Hansen 2015). In spite of this striking difference in prevalence and risk between male and female subjects, the gender difference studies are only partially considered in the field of neuroscience, since researchers typically favor male mice rather than female mice in their studies, with a ratio of 5.5 to 1 (Zucker e Beery 2010). This disproportion does not consider the gender statistical differences in the lifetime of many pathologies, suggesting serious implications for healthcare in women. The factors that influence the different lifetimes in PTSD vary from biological to psychological ones (Christiansen e Hansen 2015). Also in the context of whole-brain mapping, the few studies published hitherto focused only on male population (Cho, Rendall, e Gray 2017; Roy et al. 2022; Vetere et al. 2017; Wheeler et al. 2013; Bonapersona et al. 2022).

Here, we present BRANT, a new pipeline for whole-brain mapping, exploiting TRAP mice, high-resolution LSM and automated image processing. Using BRANT, we analyze whole-brain evolution of neural circuits involved in aversive memory in both genders. We find strong sexual dimorphism in the evolution of whole-brain networks underlying fear memory, both at the level of activation patterns and of functional connectivity.

RESULTS

1. BRANT enables scalable, high-resolution analysis of neuronal activity patterns in behaviorally-relevant cohorts

Any method aiming at complementing behavioral analysis with physiological or anatomical data must be applicable to dozens of samples, allowing its use in a statistically significant number of animals for each behavioral group. With this important constraint in mind, we developed BRANT, a scalable and user-friendly pipeline for 3D analysis of whole-brain activation patterns, that combines FosTRAP transgenic strategy (Guenthner et al. 2013), CLARITY/TDE (Costantini et al. 2015), high-resolution

RAPID-enabled LSM (Silvestri et al. 2021) and 3D automated data analysis (Frasconi et al. 2014) (**Fig.1**). BRANT was validated using a classical paradigm, as step-through passive IA. After the behavioral task, mice are injected with 4-hydroxytamoxifen (4-OHT) to drive Cre-mediated recombination in cFos-expressing neurons (Guenthner et al. 2013).

Importantly, since the reporter fluorescent protein (tdTomato) is not confined to the soma but is expressed in the entire neuron, high-resolution imaging is required to disentangle dense environments (**Fig.1**). To this aim, 3D whole brain reconstructions were then achieved by optimizing clearing and imaging protocols. All brains were made optically transparent using a modified CLARITY/TDE protocol allowing moderate expansion of tissue (27% linearly) (Di Giovanna et al. 2019). This isotropic change in sample size offered the possibility to investigate smaller components, such as neuronal processes. Samples were then imaged using a custom-made LSM with confocal line detection, able to reconstruct mesoscopic samples with microscale resolution (Müllenbroich et al. 2015). Through a system for real-time stabilization of light-sheet alignment, called RAPID, we were able to maintain the high-resolution across the entire sample volume (Silvestri et al. 2021). Since RAPID operates simultaneously with image detection, no acquisition overhead is introduced.

Each brain reconstruction comprises about 16 TeraBytes of raw data with a voxel size of 0.65x0.65x2 μm^3. The acquired datasets were stitched using ZetaStitcher (https://lens-biophotonics.github.io/ZetaStitcher/), a custom-made Python software for large volumetric stitching specifically developed for light-sheet microscopy. An important feature of ZetaStitcher is VirtualFusedVolume, an application programming interface (API) that provides seamless and effective access to high-resolution data by simply providing the spatial coordinates of the sub-volume of interest within the virtually fused volume. In this way, large volumes can be programmatically processed in smaller chunks in a distributed environment and without user intervention, a key requirement to process the large datasets produced by high-resolution LSM. Fluorescently labeled, activated neurons were detected using BrainCell Finder (Frasconi et al. 2014). This 3D automated analysis relies on a deep learning approach, based on a U-net architecture, widely used in the image-analysis field (Ronneberger, Fischer, e Brox 2015) to recognize specific structures in complex data sets. Indeed, since TdTomato is expressed also in neuronal processes, the application of standard

methods based on thresholds and blob detectors is not feasible. The task of our U-net is to transform raw images, containing many disturbing objects (like axons, dendrites, and vessels), into ideal images that include only small spheres at the location of neuronal bodies. In the images transformed by the U-net, a basic blob detector algorithm can then effectively localize the fluorescent cell bodies. The performance of this method was evaluated on 19'166 manually labeled cells, obtaining precision = TP/(TP+FP) equal to 0.80, recall = TP/(TP+FN) 0.64 and F1-score = 0.71. F1 is defined as the harmonic mean of precision and recall, 1/F1 = (1/P + 1/R)/2. To compare cell counts across multiple subjects, 3D brain datasets are spatially aligned to the Allen Brain Reference Atlas using Advanced Normalization Tools (ANTs) (Avants et al. 2011). Differently from previous reports, we did not acquire a secondary channel for atlas registration, but applied a strong gamma correction to reduce the contrast between tissue autofluorescence and the signal from fluorescent protein. We found a good registration accuracy (about 0.3 mm, see Methods), with the added value of avoiding duplicating the data size. Of note, all brain areas were included and grouped for this study, selecting 45 macro areas. We decided to use larger areas (the Allen Reference Atlas has more than 1'000 subregions) based on the measured registration accuracy, to avoid misassignment of cells.

In conclusion, the combination of high-resolution imaging and 3D analysis for processing sub-cellular information became the core of this pipeline, enabling high performance.

2. BRANT analysis reveals sexually dimorphic patterns of brain activation in different phases of aversive memory

BRANT was then applied to study the time evolution of fear memory. In order to answer our biological question, we used the step-through IA as a behavioral paradigm in which mice learn to associate a particular context (i.e. white/black box) with an aversive event (i.e. a mild foot shock). Differently from the standard CFC, IA implies decision-making since mice can decide whether to step through into the dark compartment when they are retested (Izquierdo, Furini, e Myskiw 2016). Indeed, the latency time is used as a direct measurement of memory **(fig. 2A)**. This task produces robust memory that is easily quantifiable and long-lasting only with a single training session. By using IA, we selected our three experimental groups based on the three different memory phases able to describe the

evolution of fear memory, from encoding to retrieval: *training group* was selected to study fear encoding while test *24 hours* (24h) and *7 days* (7d) after training *groups* were selected respectively to explore the recent and long-term fear retrieval. At the behavioral level, there was no significant difference in training performances in any group examined or between various test groups **(fig. 2B)**. However, latency times of training groups were significantly different compared with the latency times of the respective test groups. These differences were more significant in female classes (2- way ANOVA, followed by Bonferroni's post-hoc comparisons tests, $p < 0.01$) than the male ones (2- way ANOVA, followed by Bonferroni's post-hoc comparisons tests, $p < 0.05$) **(fig. 2B)**, indicating that all mice formed a memory trace of the training experience even though the shock intensity (0.3 mA) was weaker than the classically used (Canto-de-Souza e Mattioli 2016; Benetti et al. 2015).

Although the results from IA did not highlight any differences between male and female groups, the quantification of activated neurons (cFos) in 45 brain regions (for complete listing of brain regions, see **Supplementary Table**) revealed a strong sexual dimorphism in the assessment of fear memory. To obtain a statistically robust comparison of the activation patterns between the different phases, we performed mean-centered partial least squares analysis (PLS) (Krishnan et al. 2011). This method identifies a set of latent variables ('contrasts') in the space formed by the different experimental conditions, and a corresponding set 'saliences', i.e. the contribution of different brain areas in differentiating the samples between the different contrasts. Notably, differently from pairwise comparison of cell counts between different experimental classes, this method does not require correction for multiple sample comparisons, resulting in overall higher statistical power (Krishnan et al. 2011).

The first PLS contrasts vector has a similar structure for both genders and revealed distinct patterns of cFos expression in the training group vs. both test groups (test 24 h and test 7 d after training, **Fig. 2C-2D**). Conversely, the associated salience vectors show a distinct sexual dimorphism, as the brain areas recruited for fear encoding significantly differ between genders. In the cerebral cortex, male mice showed increased cFos expression in posterior areas (TEa, ECT and PERI) while female mice in anterior ones (ACA, PL, ORB and AI). The components of the first PLS contrast vector show higher significance in almost all brain regions of male mice, highlighting less variability between

subjects. The second PLS contrasts vector encodes difference in cFos activation between the two test groups **(Fig. 2E-2F)**. In detail, 7 days after training, male mice showed more activation in regions like SAMY, FRP, SS and VIS. Conversely, female mice were associated with increased cFos expression in PA during the training session. ME shows similar behavior in both genders, i.e. a higher activation at 7d compared to 24h. These data indicate that males and females activate, on average, different neuronal patterns in distinct phases of aversive memory, highlighting a strong sexual dimorphism which is, notably, not appreciable from behavioural data.

3. Different brain areas correlates with behavior in males and females

BRANT application showed how circuitry patterns involved in fear memory differ in male and female mice. The results obtained by PLS, based on neuron quantifications in each brain region, showed the areas which account more for the difference in activity averaged across experimental groups, each one corresponding to a specific memory phase. Thus, this analysis highlights variations between different experimental classes at population level, but is not appropriate to investigate the inter-subject variability inside the same experimental group. Indeed, latency times were significantly scattered, underlining variable behavioral responses between different mice (**Fig. 2A**). To investigate whether neuronal activation of specific areas can be accounted for the behavioral variability observed, we performed a cross-correlation analysis between regional counts and latency times (**Fig.3**), identifying strong correlation or anti correlations ($p<0.01$) for different areas in different experimental classes. In line with literature of male mice studies, the brain areas more correlated with the exploration time at training are: RHP, relevant for specific contextual information (Bucci e Robinson 2014), SAMY, which support affective evaluation and learning (Fareri e Tottenham 2016) and PVZ that is an important autonomic control center in response of stress exposure (Herman e Tasker 2016). Latency times during test sessions are usually considered in IA a measure of fear retention (Izquierdo, Furini, e Myskiw 2016). For male mice, times measured at 24h show strong correlation with CLA and BLA activity, two areas that are well known to be involved in fear (Fareri e Tottenham 2016; Hoffman et al. 2014; Sacchetti et al. 2002; Kitanishi e Matsuo 2017), but also with LSX, FRP, MO and VISC. This finding confirms the involvement of LSX in memory and emotional responses: indeed previous reports show that this region is activated during aversive situations

(Pezzone et al. 1992; Beck e Fibiger 1995; Duncan, Johnson, e Breese 1993) and projects to brain regions involved in the behavioral and cardiovascular responses to aversive stimuli (LeDoux et al. 1988). While the correlation of latency times with FRP activation seems in line with the known role of this prefrontal region in decision making (Lv et al. 2021), the involvement of MO and VISC seems less obvious. However, a recent study has proved that the motor cortex is involved in olfactory decisions (Wu et al. 2020).

Latency times 7 days after training show strong correlation with BLA, PERI and ECT, confirming our previous finding that male mice recruit more preferentially posterior rather than anterior associative areas. Interestingly, CLA and HIP are characterized by a distinct anti-correlation with behavior.

Female subjects show a completely different pattern of correlation with behavior. At training, exploration time is significantly correlated with activation of PTLp, while a clear anticorrelation is found with MO, SS, PALc, LZ and PVR. On the other hand, 7 days after training, latency times are well correlated with VISC and ORB acquisition. PTLp has an integrative function and participates in sensory and spatial processing, and decision-making. Instead, VISC generally regulates the visceral responses to threat and stress (Krushel e van Der Kooy 1988). Notably, no significant correlation between regional activation and behavior was found in female subjects tested 24h after training.

Interestingly, during fear encoding, both males and females present a strong anticorrelation between PALc, while PVR and LZ show an opposite trend between genders. A recent study demonstrated the role of pallidum in threat signaling through the inhibition of firing in presence of a danger (Moaddab, Ray, e McDannald 2021). Here, the two hypothalamic nuclei played two different roles although the hypothalamus is a central node of freezing, and sympathetic activation, necessary for survival (Burdakov e Peleg-Raibstein 2020). Pearson correlation analysis revealed a subset of activated areas depending on behavioral, that differed from male and females. This correlation allowed to appreciate the distinct activation patterns at the level of a single subject.

4. Network analysis shows strong dimorphism in the evolution of functional connectivity

Widely accepted theories affirm that memory is distributed across multiple brain regions that are functionally connected (Roy et al. 2022). To estimate average functional connectivity in different classes, we performed a Pearson cross-correlation analysis between activation counts of different brain areas, among subjects of the same experimental group. Considering only the correlations with

$p < 0.05$, we identified a network of brain areas that are co-activated in distinct phases of memory (**Fig.4**). Thus, brain areas are the nodes of this network, whilst the edges represent putative functional connections identified by super-threshold cross-correlation.

The generation of the fear memory network showed distinct evolutions in activity both comparing experimental groups and genders. These network graphs highlighted a strong gender dimorphism (**Fig. 4A**). Indeed, this evident difference was then analyzed comparing male and female functional patterns. The average connectivity was similar for our two training groups ($p<0.01$, student paired t-test, n=45) but drastically changed for all test experimental classes ($p<0.0001$, student paired t-test, n=45; **Fig. 4B**). A further analysis of the single macroregions confirmed the previous results of the average connectivity, showing how at 24 hours and 7 days time-points the functional connectome was different between the sexes (**Fig. 4C**) Basically this analysis revealed a strong increase of connectivity 24 hours after the foot shock when mice are re-exposed to the same environment. However, 7 days after training, these networks were reorganized: a strong connectivity pattern was preserved in females while male revealed a strengthening of functional connections between cortical regions, enduring in the isocortex regions.

Furthermore, this difference was confirmed by the involvement of different nodes of the networks. The role of nodes in the network was assessed by measuring its degree and betweenness. Degree of a node is the number of connections it has with the other nodes in the network, whereas betweenness is defined as the probability of finding the node in the shortest path between any randomly chosen couple of nodes in the network. In other words, the degree is a direct measure of the influence of the node in the network (the higher the degree, the more the activity of the node correlates with that of other nodes), whilst the betweenness states the importance of the node for connectivity (if a node with high betweenness is removed, many paths between other nodes are cut). Interestingly, we found that the pallidum (more precisely the PALm) acts as a network hub at training for both male and female mice. On the other hand, we observed that in the male training network the degree is higher in posterior associative areas (ECT, PERI, PTLp, in line with the PLS results shown before) and in the lateral amygdala, whereas the female training network hubs are mostly located in the striatum and in the visual cortex. The networks at test 24h are so interconnected that it is difficult to affirm that one or more specific regions act as a hub. Conversely, we note that the

thalamus is one of the few areas to be poorly connected with the rest of the brain during retrieval. Moreover, in line with literature, it negatively correlates with other brain regions at 7 days after training (Wheeler et al. 2013). In the male network at this time-point, the nodes with the highest connectivity are located in the cortex, notably in the anterior rather than posterior associative areas, suggesting a migration of the cortical fear-processing circuit. In the females, the network at test 7d is quite similar to the one at 24 hours after training, showing again high average connectivity and a disconnection of the thalamus. However, this functional connectome is also described by betweenness. Brain regions that are important central hubs in networks, differ from those that are highly ranked in betweenness (**Fig. 5**). Indeed, networks with elevated hub numbers are those with little betweenness nodes. It is interesting how in the female training group BLA have the higher betweenness centrality, even though the female average network is comparable to the male one. At 24 h after training, since the network is highly interconnected, the average betweenness is quite low, suggesting that no regions facilitate paths between two different hubs. However, during the fear retrieval, we observe that male network is characterized by many important betweenness nodes as ORB, SS, CB AND BMA (**Fig. 4B**).

DISCUSSION

Memory, as many other cognitive processes, involves complex neuronal circuits that are distributed across the entire brain and change with time (Herry e Johansen 2014). Thus, from a technical perspective, it is important to have tools that allow scalable, unbiased and quantitative analysis of brain activity at organ level yet with single-cell resolution. The classical procedure to reach this aim consists in serial sectioning of the tissue, immunostaining against cFos (or another IEG), and analysis of tissue slices (Kim et al. 2015). Although this protocol has been exploited to characterize the networks recruited during contextual (Wheeler et al. 2013) or tone fear conditioning (Cho, Rendall, e Gray 2017), it requires a massive amount of work to process each murine brain, thus resulting impractical for routine use in many laboratories. Automated 3D imaging, such as serial two-photon sectioning (STP) (Ragan et al. 2012) and light-sheet microscopy (Mertz 2011) emerged in the last decade as a potential game changer for whole-brain analysis at cellular level, and indeed it has been exploited to map neuronal activation in different contexts (Renier et al. 2016; Kim et al.

2017), including fear memory (Roy et al. 2022; Bonapersona et al. 2022). However, STP is usually employed in a sampling scheme, failing to cover the entire tissue volume (Kim et al. 2017). On the other hand, LSM-based pipelines, like ClearMap, are typically limited to a resolution of several µm per voxel, preventing their use in densely labeled regions (**Fig. 1**). Here, we presented BRANT, a combination of high-resolution LSM and scalable computational analysis. On the optics side, the use of RAPID autofocusing guarantees high contrast and resolution across the entire sample (Silvestri et al. 2021). On the image processing side, the architecture provided by ZetaStitcher allows programmatic access to extra-large tissue volumes (several TeraVoxels) for subsequent quantification. Importantly, BRANT is based on fully open-source software, and can thus be used and improved by the entire community in a collaborative spirit.

The lack of scalable methods for whole brain mapping has limited the analysis of brain-wide activation patterns in fear memory to a handful of studies (Cho, Rendall, e Gray 2017; Tonegawa, Morrissey, e Kitamura 2018; Bonapersona et al. 2022; Vetere et al. 2017; Wheeler et al. 2013). Most reports about fear memory refer to one or few nuclei or areas. Consequently, the obtained results are specific to those neuronal regions, which in turn makes it difficult to form an overview when integrating the data together. Indeed, small changes of experimental setting (from the behavioural task to the age and sex of animals) can lead to contrasting outcomes, making it difficult to obtain a comprehensive view of brain circuits underlying memory formation, consolidation and retrieval. Additionally, this problem is even more accentuated considering the limited literature about female subjects and gender differences. Indeed, the majority of previous studies about gender dimorphisms have mainly highlighted differences in brain anatomy (Kim et al. 2017; Bayless e Shah 2016; Simerly 2002; Cachero et al. 2010) and in cellular physiology (Florido et al. 2021). The identification of these anatomical or molecular differences is a useful starting point for the comprehension of neural circuits underlying gender-specific behaviors. Our current study demonstrated how fear response required the recruitment of sex-different networks. It is noteworthy how this difference is emphasized during the 7d retrieval, suggesting that female mice require more time to move the fear neuronal network towards cortical circuits. Moreover, in agreement with previous reports about sex differences, we also notice an opposite enrollment of brain areas classically involved in hormone control such as PVR (Yang e Shah 2014; Florido et al. 2021). During training, this area correlates with behavior in

males and anti-correlates with females (**Fig.3**). This is a proof of concept of how hormonal response differently influences the consolidation of fearful events, leading to a divergent evolution of memory. Considering that many neuro-psychiatric disorders exhibit sex differences in lifetime prevalence (Bangasser e Valentino 2014; Smith e Dahodwala 2014; Werling e Geschwind 2013; Davies 2014; Li e Singh 2014), this study could pave the way for a better understanding of these outcomes.

Here, BRANT was applied to understand the time-evolution of brain circuits underpinning fear memory in the IA paradigm with a mild footshock. Due to the limited number of whole- brain studies about fear memory, comparing our results with previous reports (Wheeler et al. 2013; Cho, Rendall, e Gray 2017) is not straightforward because fear memory can be assessed in rodents by using diverse behavioral tasks. Indeed, the IA behavioral paradigm presented here might recruit a different circuitry with respect to context or auditory fear conditioning, since decision-making by the animals - which have to choose to step through the gate towards the dark compartment - is an important component, absent in the above mentioned paradigms. In addition, using a mild footshock (0.3 mA), we explored an aversive rather than traumatic memory.

In this fragmented context - both on the brain region studied and on the behavioral task used - the scalable and comprehensive analysis enabled by BRANT can play an important role. Indeed, this open-source pipeline offers the possibility to perform whole-brain activation analysis at high throughput, allowing cell-resolution brain mapping on behavioral cohorts. Here, this method highlighted a sexual dimorphism in the evolution of fear memory but it is readily adaptable for broader applications such as drug discovery or other biological purposes. The advantage of using micrometer resolution on a brain-wide scale and 3D automated analysis could revolutionize the way of studying brain connectivity and functions.

METHODS

ANIMALS

Male and female FosTRAP mice (B6.129(Cg)-Fos$^{tm1.1(cre/ERT2)Luo}$/J × B6.Cg-Gt(ROSA)26Sor$^{tm9(CAG-tdTomato)Hze}$/J) were used for this work (Guenthner et al. 2013). They were housed in groups, giving the opportunity to behave as 'social animals'. Mice received food and water ad libitum and were maintained in a room under controlled light and dark cycle (12/12 h; light starts at 7:00 AM), temperature (22 ± 2 °C), and humidity (55 ± 10 %). Adult mice (aged between 3 months and 6 months) were divided in three groups: training (n=6 males, n=4 females), test 24h (hours) (n=5 males, n=6 females) and test 7d (days) (n=4 males, n=4 females). All experimental procedures were approved by the Italian Ministry of Health (Authorization n. 512-2018_FC). Alternatives to in vivo techniques were not available, but all experiments were conducted according to principles of the 3Rs.

BEHAVIORAL TASK

All mice were trained and tested using the behavioral paradigm, step-through inhibitory avoidance (IA). Behavioral procedures were performed in a sound-attenuated room, during the light cycle. The day before the experiment, mice were placed in this room for habituation. Each mouse was subjected to the task separately, and care was taken to remove any olfactory tracks of previous experiments by cleaning the box. The apparatus consists of an automatic controller and a box (47x18x25(h)cm, Ugo Basile, Comerio, Italy) which is divided into two separate compartments by a sliding door. The start compartment is brightly-illuminated while the escape one is dark and connected to the shocker. During the training session, every mouse was gently placed in the brightly-illuminated compartment, facing the door and allowing free access to the dark compartment. The apparatus is designed to exploit the natural behavior of mice to go into the darkness. For this reason, they rapidly step through the door and then received a 0.3 mA mild foot-shock lasting 2 s. Latency was measured using an automated tilting-floor detection mechanism. After the foot-shock, mice were immediately removed from the dark box, and consequently, they received the 4-TMX injection. The retention test was carried out 24 h or 7 d after the training session. All mice were trained, and a part was tested 24h after training while the other, 7 d after. During the test, trained animals were placed again on the start compartment until they eventually enter into the dark one. The procedure was the same, but mice do not receive any shock during this phase. Five minutes is the maximal latency time given for stepping through, and it is measured by the same automated mechanism. At the end of 300 s, mice, that do not step through, are removed from the apparatus. After removal from the system, all animals received the 4-TMX injection. The latency to step through was considered a direct measurement of memory.

DELIVERY OF 4-OHT

Mice were handled and got used to needle pain with saline solution daily for at least 3 days prior to the 4-OHT injection. 4-OHT (Sigma H6278) was first dissolved in absolute ethanol to give a final concentration of 20 mg/mL. This stock was then mixed with corn oil (Sigma C8267) at 37 °C in order to get an emulsion. The injectable oil formulation at the final concentration of 50 mg/kg was obtained using the Eppendorf ThermoMixer® C. The emulsion was heated and shaken for 2 hours until the ethanol was entirely evaporated. At this time, the drug was totally dissolved in corn oil and kept at 37°C. 4-TMX was delivered by intraperitoneal (i.p.) injection through an injection needle 22 gauge.

EX-VIVO PROCESSING AND CLARITY

One week after the tamoxifen injection, animals were deeply anesthetized isoflurane (1.5%–2%) and transcardially perfused with 50 mL of ice-cold 0.01 M phosphate buffered saline (PBS) solution (pH 7.6), followed by 75 mL of freshly prepared paraformaldehyde (PFA) 4% (wt/vol, pH 7.6). Brains were extracted and prepared according to the CLARITY/TDE protocol (Chung et al., 2013; Costantini et al., 2015). Immediately after perfusion, brains were post-fixed in PFA overnight at 4°C. The day after, samples were incubated in a hydrogel solution (containing 10% acrylamide (vol/vol), 2.5% bis-acrylamide (vol/vol) and 0.25% VA044 (wt/vol) in PBS) at 4°C for 3 days, allowing a sufficient diffusion of the solution into the tissue. Samples were then degassed, replacing oxygen inside the vials with nitrogen, and incubated in a water bath at 37°C for 3 hours in order to initiate polymerization of the hydrogel. After 3 hours, embedded brains were placed in a clearing solution (containing 4.4 % (wt/vol) sodium dodecyl sulfate (SDS) and 1.2 % (wt/vol) boric acid in ultra-pure water, pH 8.5) at 37°C. Clearing solution was changed every 2-3 days. Specimens were gently shaken throughout the whole clearing period, which typically takes 3-4 weeks. When the samples appeared sufficiently transparent, they were incubated 1 day in PBS with 0.1 Triton-X (PBST, pH 7.6) and 1 day in PBS (pH 7.6), removing the excess SDS. Finally, murine brains optically cleared with serial immersions of mixtures containing 20% and 40% 2-2' Thiodiethanol (TDE) in PBS, each for 1 day while rotating. The last mixture (40% TDE) was used as an index-matching solution for our imaging(Di Giovanna et al., 2019).

LIGHT-SHEET MICROSCOPY

The custom-made light-sheet microscope, exploiting RAPID autofocusing, has been described in detail in references (Müllenbroich et al. 2015; Silvestri et al. 2021). In brief, the sample is illuminated from the side using a virtual light sheet created with a galvanometer scanner (6220H, Cambridge Technology), coupled via a 4f system to an air objective (Plan Fluor EPI 10X NA 0.3, Nikon) covered with a protective coverslip. Light emitted from the specimen is detected orthogonally to the illumination plane using an immersion objective corrected for clearing solutions (XLPLN10XSVMP 10X NA 0.6, Olympus). Then, it is bandpass-filtered to isolate fluorescence light and projected by a

tube lens onto the chip of a scientific complementary metal-oxide-semiconductor (sCMOS) camera (Orca Flash 2.0, Hamamatsu) operating in rolling-shutter mode to guarantee confocal line detection. During imaging, the sample was fixed in a refractive index-matched quartz cuvette (3/Q/15/TW, Starna Scientific) and moved using a set of high-accuracy linear translators (M-122.2DD, Physik Instrumente). Sample-induced defocus is measured in real-time using RAPID (Silvestri et al. 2021), and correction was implemented by moving the objective with an additional linear translation stage (M-122.2DD, Physik Instrumente). The entire system was controlled by custom software written in C++, available at https://github.com/lens-biophotonics/SPIMlab.

IMAGE ANALYSIS

Tiled images acquired with LSM were stitched together using ZetaStitcher (https://github.com/lens-biophotonics/ZetaStitcher). As well as generating a low-resolution view of the entire imaging volume, this software includes an application programming interface (VirtualFusedVolume) to access the high-resolution volume. Image were then visualized using FIJI/ImageJ (https://fiji.sc).

WHOLE-BRAIN CELL DETECTION

Fluorescently labeled neurons were localized in the whole-brain images using BrainCell Finder (Frasconi et al. 2014) (https://github.com/lens-biophotonics/BCFind). In brief, patches of the original dataset (accessed via VirtualFusedVolume) were fed into a UNet with four contraction layers of 3D convolutions with an exponentially increasing number of filters, and four expansion layers of transposed 3D convolutions with a decreasing number of filters. UNet training was carried out with binary cross-entropy loss and Adam optimizer. The goal of this network is to perform semantic deconvolution, that is, to transform the original image into an ideal one in which cell bodies are clearly visible, while other structures such as dendrites and axons are removed. The network was previously trained on a ground-truth dataset in which a human expert has localized the centers of neuronal somata. The training dataset was composed of 221 image stacks for a total volume of approximately 6.8 mm^3 and 19’166 manually labeled cells. The stacks were randomly selected from different samples and different areas of the brain, to train the network to recognize the large variability in cell shape that can be found across the sample. The images deconvolved by the network are then processed with a standard blob detection algorithm (difference of Gaussians, DoG) to identify the center of bright structures, which in this case are the neurons. The overall performance of the method is evaluated by comparing the list of neuron centers found by the software with the human-annotated ground-truth test set of 57 image stacks for a total volume of approximately 1.8 mm^3 and 1’786 manually labeled cells. Again, these stacks were randomly selected from different samples and different areas of the brain, to test network performance in different contexts. If two neuron centers from the two annotations (automatic and manual) are closer than 10 µm (approximately half of the average diameter of a neuron), they are considered to be the same cell, that is, a true positive (TP). If a center is present only in the manual annotation, it is considered a false negative (FN), whereas

if it is present only in the results of the algorithm, it is considered a false positive (FP). The counting of true positives, false positives and false negatives was carried out using the maximum bipartite matching algorithm34. We evaluated localization performance using the formulas precision = TP/(TP + FP) and recall = TP/(TP + FN), and the F1-score, which is defined as the harmonic mean of precision and recall. For our test set, the precision was 0.80, the recall was 0.64 and the F1-score was 0.71. All annotations of cell positions were performed using Vaa3D (https://github.com/Vaa3D).

SPATIAL REGISTRATION TO ATLAS

A downsampled version of the whole-brain dataset (voxel size, 25 μm) was spatially registered to the Allen reference atlas using Advanced Normalization Tools (Avants et al. 2011), with a sequence of rigid, affine and diffeomorphic (that is, symmetric normalization) transformations. The same transformations were applied to the point clouds produced by the BrainCell Finder, to represent the position of activated neurons. Each cell was then assigned to a selected brain area based on its position. To evaluate registration accuracy, 10 reference points were manually marked in 10 different aligned brains and in the reference atlas. Then, the Euclidean distance between couples of corresponding points (samples vs atlas) was calculated for each point and each sample (100 measures in total). The root-mean-square average value of the distance (0.30 +/- 0.08 mm, mean +/- s.d.) was considered as the alignment error.

PLS ANALYSIS

The effect of each experimental class on regional cell counts were evaluated using Task PLS (Krishnan et al. 2011; McIntosh et al. 1996). Briefly, a dummy matrix with as many columns as the number of subjects and as many lines as the experimental classes where designed, with 1 in the matrix elements corresponding to the right matching subject-class and 0 elsewhere. This was multiplied by the regional count matrix (as many lines as the subjects, as many columns as the brain areas analyzed), and the product was processed using singular value decomposition. The resulting left and right matrices contained the contrasts and the saliences, respectively. These identify latent variables in the spaces of experimental classes and in the space of cell counts that best explain the variability observed in the data. Statistical error was calculated using bootstrap technique by resampling 1000 times with replacement. The reported saliences are the raw ones divided by the standard deviation of the bootstrap results, and can thus be interpreted as z-values. In this sense, the dashed lines in Fig.2 represent different significance levels ($p < 0.1$, $p < 0.05$, $p < 0.01$).

FUNCTIONAL NETWORK CONSTRUCTION

The inter-regional correlation (Wheeler et al. 2013) was calculated for each group of mice in order to quantify the co-variation of activated cell counts in 45 brain regions across mice of the same group. The functional connections between different regions were identified by imposing a suitable

threshold for the inter-regional correlation. The threshold was properly defined to identify cross-correlations with a p-value of less than 0.05. Starting from the correlation matrix and the given threshold value, the corresponding adjacency matrix was computed for each group of mice. Each adjacency matrix defines a corresponding network where the nodes are the 45 brain regions and the links are the functional connections between the regions: positive links correspond to excitatory functional connections and negative links to inhibitory functional connections. The Degree centrality of the nodes was calculated by counting the number of connections of each node without considering the sign of the connections, and was normalized on the maximum number of potential connections (44). The betweenness centrality was calculated by means of the algorithm betweenness_centrality of the Python package networkx based on (Brandes 2001; 2008; Freeman 1977).

FIGURES

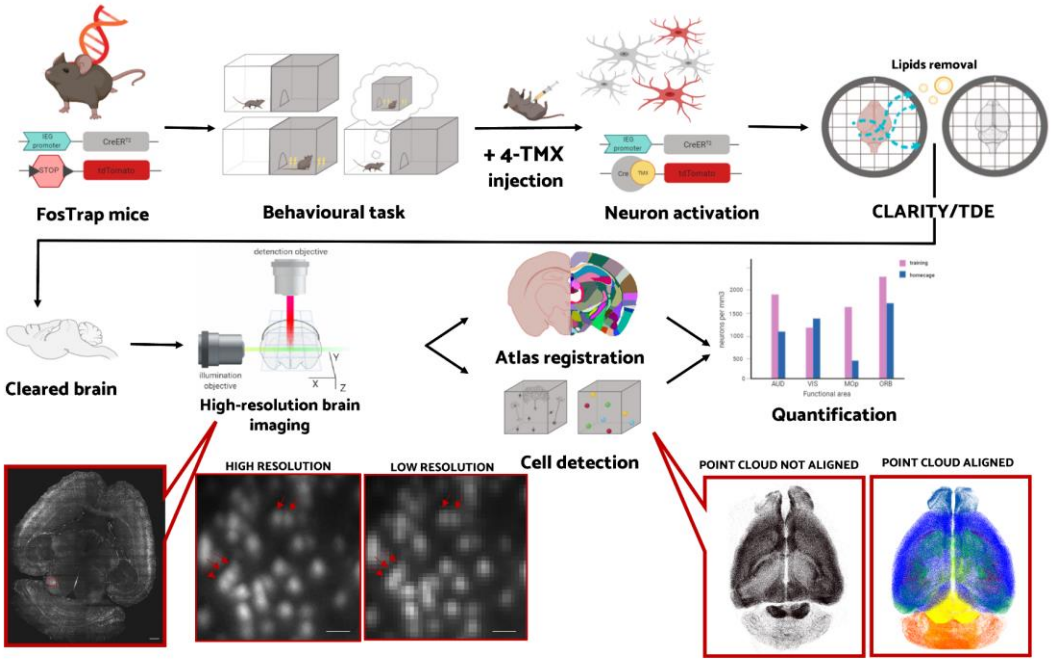

***Figure 1*: Experimental pipeline**. Schematic representation of various steps constituting the experimental pipeline. FosTrap mice underwent the step-through IA task. Injecting 4-OHT, activated neurons permanently expressed tdTomato fluorescent proteins. After perfusion, all brains were processed with CLARITY/TDE protocol and imaged with a high-resolution RAPID-enabled LSM. High resolution imaging was fundamental for cell detection and for 3D automated analysis. All brains were registered to the Allen Brain Atlas. All activated neurons were detected and quantified.

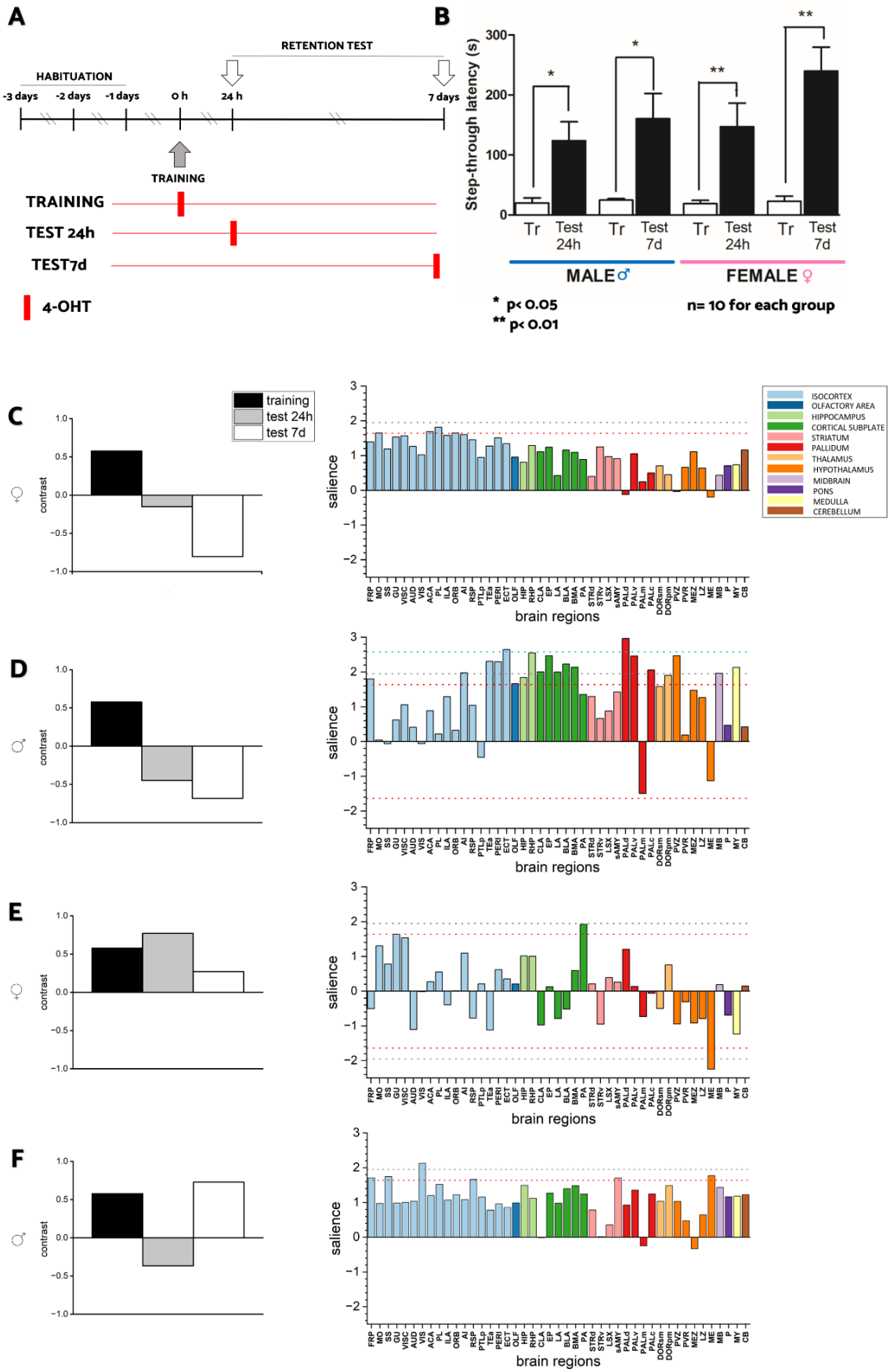
A
RETENTION TEST
HABITUATION
-3 days
-2 days
-1 days
0 h
24 h
7 days
TRAINING
TRAINING
TEST 24h
TEST7d
4-OHT
B
Step-through latency (s)
300
200
100
0
Tr
Test 24h
Tr
Test 7d
Tr
Test 24h
Tr
Test 7d
MALE♂
FEMALE♀
* p< 0.05
** p< 0.01
n= 10 for each group
C
training
test 24h
test 7d
contrast
salience
brain regions
ISOCORTEX
OLFACTORY AREA
HIPPOCAMPUS
CORTICAL SUBPLATE
STRIATUM
PALLIDUM
THALAMUS
HYPOTHALAMUS
MIDBRAIN
PONS
MEDULLA
CEREBELLUM
D
E
F

Figure 2 **: Behavioral task and PLS analysis.** (A) The schematic drawing shows the sequence of procedures. Animals are handled for three days before training. During the training session, all mice receive a foot-shock. Test is performed 24h or 7 days after training. By the 4-OHT injection at three time points, mice were divided in three experimental classes: training; test 24h, test 7d (B) The comparisons of acquisition and retention latency times are analyzed by 2-way ANOVA, followed by Bonferroni's post-hoc comparisons tests. Data are expressed as means ± SEM of 4 to 6 animals for each group. (C-F) Task PLS analysis of cFos expression in trained vs. tested 24h or 7d after training. These analyses identified two contrasts (left graph) that strongly differentiated the trained vs.tested conditions for female (C, E) and male (D, F) mice. Salience scores, normalized by standard deviation calculated with bootstrap (right), identify regions that maximally differentiate between these conditions. The red, gray and blue lines reflect respectively a salience score of 1.64 ($p<0.1$), 1.96 ($p<0.05$) and 2.58 ($p>0.01$).

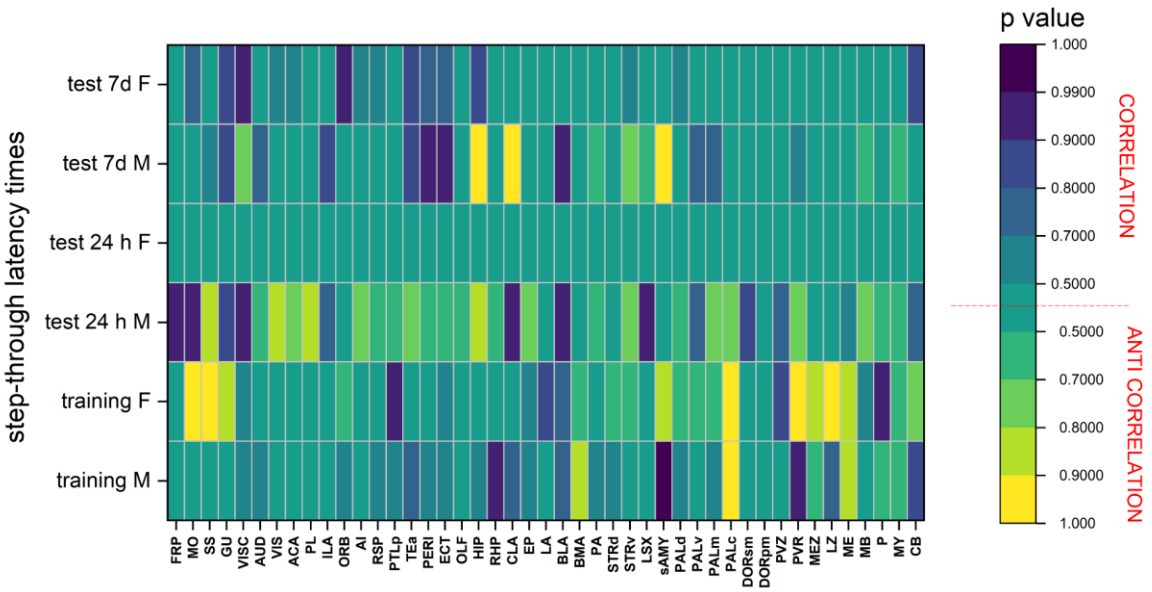

Figure 3. **Effect of behavior on brain region activations** Pearson correlation heat maps. Here heat maps represent the correlation between the number of cFos^{+} neurons in each region and the latency time mice spend to step-through into the dark compartment. On the right side of the plot, different colors correspond to different p values.

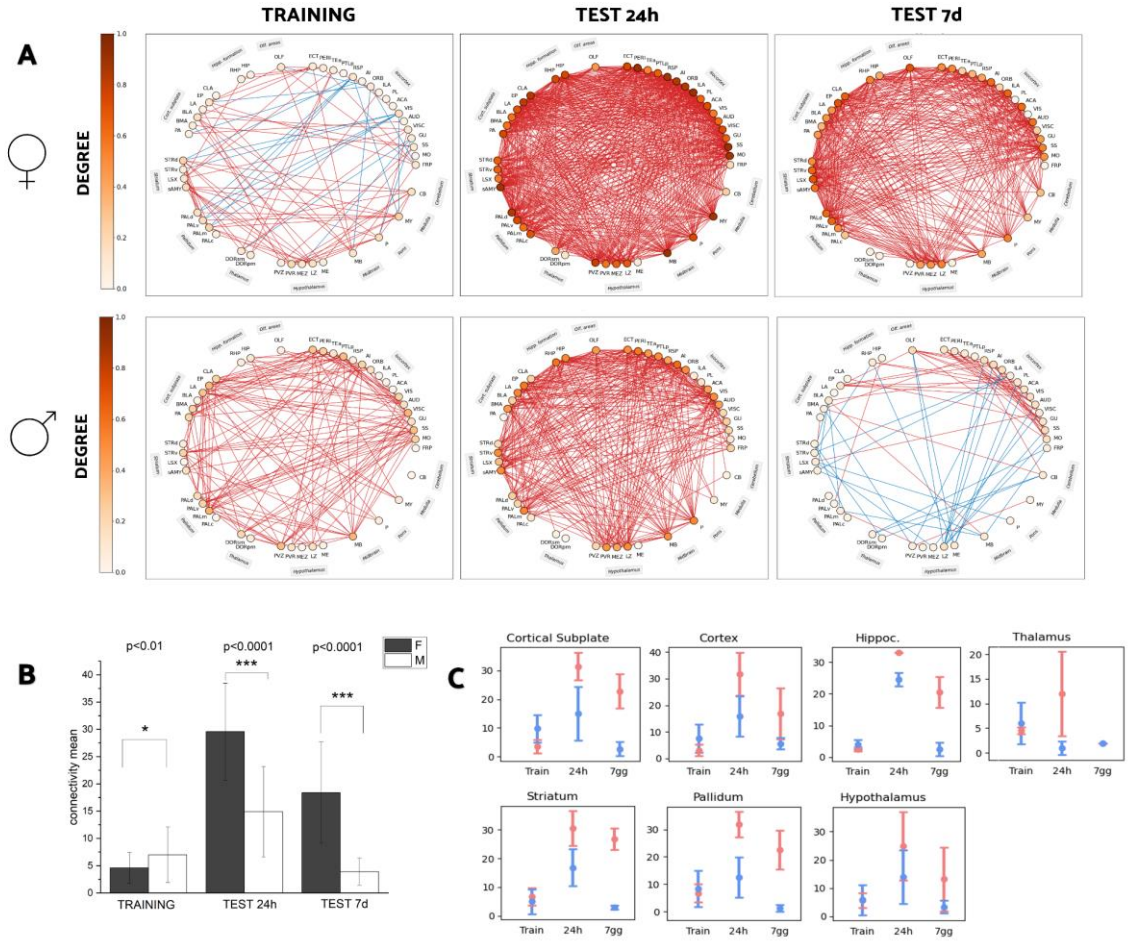

Figure 4. Fear memory networks in male and female mice. (A) Network graphs were generated by considering only the strongest correlations (see Methods). Nodes around the circle represent the 45 selected regions **(Listed in Tab**). Node color is proportional to the number of connections (degree), normalized with the highest possible number of connections (44). Darker colors correspond to higher degrees. (B) The comparison of average connectivity between genders. At training, connectivity distribution is similar between males and females while during test connectivity is higher in females compared to males. (C) Standard deviation of the average connectivity of macroregions in the three experimental classes, for both genders.

Figure 5. Betweenness of fear memory networks in male and female mice. Network graphs were generated by considering only the strongest correlations (see Methods). Nodes around the circle represent the 45 selected regions **(Listed in Tab**). Node color is proportional to the fraction of the shortest paths between any random couple of areas that pass through the selected region (betweenness). Darker colors correspond to higher betweenness.

SUPPLEMENTARY
Table- List of Brain Region

Isocortex
FRP frontal pole
MO somatomotor areas
SS somatosensory areas
GU gustatory areas
VISC visceral areas
AUD auditory areas
VIS visual area
ACA anterior cingulate area
PL prelimbic area
ILA infralimbic area
ORB orbital area
AI agranular insular area
RSP retrosplenial area
PTLp posterior parietal association areas
Tea temporal association areas
PERI Perirhinal area
ECT Ectorhinal area

OLF Olfactory areas

Hippocampal formation
HIP hippocampal region
RHP retrohippocampal region

Cortical subplate
CLA Claustrum
EP Endopiriform nucleus
LA lateral amygdalar nucleus
BLA Basolateral amygdalar nucleus
BMA Basomedial amygdalar nucleus
PA posterior amygdalar nucleus

Striatum
STRd striatum dorsal region
STRv striatum ventral region
LSX lateral septal complex
sAMY Striatum-like amygdalar nuclei

Pallidum
PALd dorsal pallidum
PALv ventral pallidum
PALm medial pallidum
PALc caudal pallidum

Thalamus
DORsm thalamus, sensory-motor
DORpm thalamus, polymodal association

Hypothalamus
PVZ periventricular zone
PVR periventricular region
MEZ Hypothalamic medial zone
LZ hypothalamic lateral zone

ME median eminence

MB Midbrain
P Pons
MY Medulla
CB Cerebellum

Disclosures
The authors declare that there are no conflicts of interest related to this paper.

Funding
This project received funding from the European Union's Horizon 2020 research and innovation programme under grant agreements n. 785907 (HBP SGA2), 945539 (HBP SGA3) and 654148 (Laserlab-Europe). The project have also been supported by the Italian Ministry for Education, University, Research through projects CNR-FOE-LENS-2021, Flag-era HA-ction, Smart Brain, and by "Ente Cassa di Risparmio di Firenze" (private foundation). Part of this work was performed in the frame of the Proof of Concept Studies for the ESFRI research infrastructure project Euro-BioImaging at the PCS facility LENS.

BIBLIOGRAPHY

Avants, Brian B., Nicholas J. Tustison, Gang Song, Philip A. Cook, Arno Klein, e James C. Gee. 2011. «A Reproducible Evaluation of ANTs Similarity Metric Performance in Brain Image Registration». *NeuroImage* 54 (3): 2033–44. https://doi.org/10.1016/j.neuroimage.2010.09.025.

Bangasser, Debra A., e Rita J. Valentino. 2014. «Sex Differences in Stress-Related Psychiatric Disorders: Neurobiological Perspectives». *Frontiers in Neuroendocrinology* 35 (3): 303–19. https://doi.org/10.1016/j.yfrne.2014.03.008.

Bayless, Daniel W., e Nirao M. Shah. 2016. «Genetic Dissection of Neural Circuits Underlying Sexually Dimorphic Social Behaviours». *Philosophical Transactions of the Royal Society B: Biological Sciences* 371 (1688): 20150109. https://doi.org/10.1098/rstb.2015.0109.

Beck, Ch, e Hc Fibiger. 1995. «Conditioned Fear-Induced Changes in Behavior and in the Expression of the Immediate Early Gene c-Fos: With and without Diazepam Pretreatment». *The Journal of Neuroscience* 15 (1): 709–20. https://doi.org/10.1523/JNEUROSCI.15-01-00709.1995.

Benetti, Fernando, Cristiane Regina Guerino Furini, Jociane de Carvalho Myskiw, Gustavo Provensi, Maria Beatrice Passani, Elisabetta Baldi, Corrado Bucherelli, Leonardo Munari, Ivan Izquierdo, e Patrizio Blandina. 2015. «Histamine in the Basolateral Amygdala Promotes Inhibitory Avoidance Learning Independently of Hippocampus». *Proceedings of the National Academy of Sciences* 112 (19). https://doi.org/10.1073/pnas.1506109112.

Bonapersona, Valeria, Heike Schuler, Ruth Damsteegt, Youri Adolfs, R. Jeroen Pasterkamp, Martijn P. van den Heuvel, Marian Joëls, e R. Angela Sarabdjitsingh. 2022. «The Mouse Brain after Foot Shock in Four Dimensions: Temporal Dynamics at a Single-Cell Resolution». *Proceedings of the National Academy of Sciences* 119 (8): e2114002119. https://doi.org/10.1073/pnas.2114002119.

Brandes, Ulrik. 2001. «A Faster Algorithm for Betweenness Centrality*». *The Journal of Mathematical Sociology* 25 (2): 163–77. https://doi.org/10.1080/0022250X.2001.9990249.

———. 2008. «On Variants of Shortest-Path Betweenness Centrality and Their Generic Computation». *Social Networks* 30 (2): 136–45. https://doi.org/10.1016/j.socnet.2007.11.001.

Bucci, David J., e Siobhan Robinson. 2014. «Toward a Conceptualization of Retrohippocampal Contributions to Learning and Memory». *Neurobiology of Learning and Memory* 116 (dicembre): 197–207. https://doi.org/10.1016/j.nlm.2014.05.007.

Burdakov, Denis, e Daria Peleg-Raibstein. 2020. «The Hypothalamus as a Primary Coordinator of Memory Updating». *Physiology & Behavior* 223 (settembre): 112988. https://doi.org/10.1016/j.physbeh.2020.112988.

Cachero, Sebastian, Aaron D. Ostrovsky, Jai Y. Yu, Barry J. Dickson, e Gregory S.X.E. Jefferis. 2010. «Sexual Dimorphism in the Fly Brain». *Current Biology* 20 (18): 1589–1601. https://doi.org/10.1016/j.cub.2010.07.045.

Canto-de-Souza, L., e R. Mattioli. 2016. «The Consolidation of Inhibitory Avoidance Memory in Mice Depends on the Intensity of the Aversive Stimulus: The Involvement of the Amygdala, Dorsal Hippocampus and Medial Prefrontal Cortex». *Neurobiology of Learning and Memory* 130 (aprile): 44–51. https://doi.org/10.1016/j.nlm.2016.01.012.

Charak, Ruby, Cherie Armour, Ask Elklit, Disket Angmo, Jon D. Elhai, e Hans M. Koot. 2014. «Factor Structure of PTSD, and Relation with Gender in Trauma Survivors from India». *European Journal of Psychotraumatology* 5 (1): 25547. https://doi.org/10.3402/ejpt.v5.25547.

Cho, Jin-Hyung, Sam D. Rendall, e Jesse M. Gray. 2017. «Brain-Wide Maps of *Fos* Expression during Fear Learning and Recall». *Learning & Memory* 24 (4): 169–81. https://doi.org/10.1101/lm.044446.116.

Christiansen, Dorte M., e Maj Hansen. 2015. «Accounting for Sex Differences in PTSD: A Multi-Variable Mediation Model». *European Journal of Psychotraumatology* 6 (1): 26068. https://doi.org/10.3402/ejpt.v6.26068.

Chung, Kwanghun, Jenelle Wallace, Sung-Yon Kim, Sandhiya Kalyanasundaram, Aaron S. Andalman, Thomas J. Davidson, Julie J. Mirzabekov, et al. 2013. «Structural and Molecular

Interrogation of Intact Biological Systems». *Nature* 497 (7449): 332–37. https://doi.org/10.1038/nature12107.
Costantini, Irene, Jean-Pierre Ghobril, Antonino Paolo Di Giovanna, Anna Letizia Allegra Mascaro, Ludovico Silvestri, Marie Caroline Müllenbroich, Leonardo Onofri, et al. 2015. «A Versatile Clearing Agent for Multi-Modal Brain Imaging». *Scientific Reports* 5 (1): 9808. https://doi.org/10.1038/srep09808.
Davies, William. 2014. «Sex Differences in Attention Deficit Hyperactivity Disorder: Candidate Genetic and Endocrine Mechanisms». *Frontiers in Neuroendocrinology* 35 (3): 331–46. https://doi.org/10.1016/j.yfrne.2014.03.003.
Di Giovanna, Antonino Paolo, Caterina Credi, Alessandra Franceschini, Marie Caroline Müllenbroich, Ludovico Silvestri, e Francesco Saverio Pavone. 2019. «Tailored Sample Mounting for Light-Sheet Fluorescence Microscopy of Clarified Specimens by Polydimethylsiloxane Casting». *Frontiers in Neuroanatomy* 13 (marzo): 35. https://doi.org/10.3389/fnana.2019.00035.
Duncan, Ge, Kb Johnson, e Gr Breese. 1993. «Topographic Patterns of Brain Activity in Response to Swim Stress: Assessment by 2-Deoxyglucose Uptake and Expression of Fos-like Immunoreactivity». *The Journal of Neuroscience* 13 (9): 3932–43. https://doi.org/10.1523/JNEUROSCI.13-09-03932.1993.
Fareri, Dominic S., e Nim Tottenham. 2016. «Effects of Early Life Stress on Amygdala and Striatal Development». *Developmental Cognitive Neuroscience* 19 (giugno): 233–47. https://doi.org/10.1016/j.dcn.2016.04.005.
Florido, A., E. R. Velasco, C. M. Soto-Faguás, A. Gomez-Gomez, L. Perez-Caballero, P. Molina, R. Nadal, O. J. Pozo, C. A. Saura, e R. Andero. 2021. «Sex Differences in Fear Memory Consolidation via Tac2 Signaling in Mice». *Nature Communications* 12 (1): 2496. https://doi.org/10.1038/s41467-021-22911-9.
Frasconi, Paolo, Ludovico Silvestri, Paolo Soda, Roberto Cortini, Francesco S. Pavone, e Giulio Iannello. 2014. «Large-Scale Automated Identification of Mouse Brain Cells in Confocal Light Sheet Microscopy Images». *Bioinformatics* 30 (17): i587–93. https://doi.org/10.1093/bioinformatics/btu469.
Freeman, Linton C. 1977. «A Set of Measures of Centrality Based on Betweenness». *Sociometry* 40 (1): 35. https://doi.org/10.2307/3033543.
Guenthner, Casey J., Kazunari Miyamichi, Helen H. Yang, H. Craig Heller, e Liqun Luo. 2013. «Permanent Genetic Access to Transiently Active Neurons via TRAP: Targeted Recombination in Active Populations». *Neuron* 78 (5): 773–84. https://doi.org/10.1016/j.neuron.2013.03.025.
Herman, James P., e Jeffrey G. Tasker. 2016. «Paraventricular Hypothalamic Mechanisms of Chronic Stress Adaptation». *Frontiers in Endocrinology* 7 (ottobre). https://doi.org/10.3389/fendo.2016.00137.
Herry, Cyril, e Joshua P Johansen. 2014. «Encoding of Fear Learning and Memory in Distributed Neuronal Circuits». *Nature Neuroscience* 17 (12): 1644–54. https://doi.org/10.1038/nn.3869.
Hoffman, Ann N., Nickolaus G. Lorson, Federico Sanabria, M. Foster Olive, e Cheryl D. Conrad. 2014. «Chronic Stress Disrupts Fear Extinction and Enhances Amygdala and Hippocampal Fos Expression in an Animal Model of Post-Traumatic Stress Disorder». *Neurobiology of Learning and Memory* 112 (luglio): 139–47. https://doi.org/10.1016/j.nlm.2014.01.018.
Izquierdo, Ivan, Cristiane R. G. Furini, e Jociane C. Myskiw. 2016. «Fear Memory». *Physiological Reviews* 96 (2): 695–750. https://doi.org/10.1152/physrev.00018.2015.
Johansen, Joshua P., Christopher K. Cain, Linnaea E. Ostroff, e Joseph E. LeDoux. 2011. «Molecular Mechanisms of Fear Learning and Memory». *Cell* 147 (3): 509–24. https://doi.org/10.1016/j.cell.2011.10.009.
Josselyn, Sheena A., e Paul W. Frankland. 2018. «Memory Allocation: Mechanisms and Function». *Annual Review of Neuroscience* 41 (1): 389–413. https://doi.org/10.1146/annurev-neuro-080317-061956.
Kim, Yongsoo, Kannan Umadevi Venkataraju, Kith Pradhan, Carolin Mende, Julian Taranda, Srinivas C. Turaga, Ignacio Arganda-Carreras, et al. 2015. «Mapping Social Behavior-Induced Brain Activation at Cellular Resolution in the Mouse». *Cell Reports* 10 (2): 292–305. https://doi.org/10.1016/j.celrep.2014.12.014.

Kim, Yongsoo, Guangyu Robert Yang, Kith Pradhan, Kannan Umadevi Venkataraju, Mihail Bota, Luis Carlos García del Molino, Greg Fitzgerald, et al. 2017. «Brain-Wide Maps Reveal Stereotyped Cell-Type-Based Cortical Architecture and Subcortical Sexual Dimorphism». *Cell* 171 (2): 456-469.e22. https://doi.org/10.1016/j.cell.2017.09.020.

Kindt, Merel. 2014. «A Behavioural Neuroscience Perspective on the Aetiology and Treatment of Anxiety Disorders». *Behaviour Research and Therapy* 62 (novembre): 24–36. https://doi.org/10.1016/j.brat.2014.08.012.

Kitanishi, Takuma, e Naoki Matsuo. 2017. «Organization of the Claustrum-to-Entorhinal Cortical Connection in Mice». *The Journal of Neuroscience* 37 (2): 269–80. https://doi.org/10.1523/JNEUROSCI.1360-16.2016.

Krishnan, Anjali, Lynne J. Williams, Anthony Randal McIntosh, e Hervé Abdi. 2011. «Partial Least Squares (PLS) Methods for Neuroimaging: A Tutorial and Review». *NeuroImage* 56 (2): 455–75. https://doi.org/10.1016/j.neuroimage.2010.07.034.

Krushel, Leslie A., e Derek van Der Kooy. 1988. «Visceral Cortex: Integration of the Mucosal Senses with Limbic Information in the Rat Agranular Insular Cortex». *The Journal of Comparative Neurology* 270 (1): 39–54. https://doi.org/10.1002/cne.902700105.

LeDoux, Je, J Iwata, P Cicchetti, e Dj Reis. 1988. «Different Projections of the Central Amygdaloid Nucleus Mediate Autonomic and Behavioral Correlates of Conditioned Fear». *The Journal of Neuroscience* 8 (7): 2517–29. https://doi.org/10.1523/JNEUROSCI.08-07-02517.1988.

Li, Rena, e Meharvan Singh. 2014. «Sex Differences in Cognitive Impairment and Alzheimer's Disease». *Frontiers in Neuroendocrinology* 35 (3): 385–403. https://doi.org/10.1016/j.yfrne.2014.01.002.

Lv, Chenyu, Qiang Wang, Chuansheng Chen, Gui Xue, e Qinghua He. 2021. «Activation Patterns of the Dorsal Medial Prefrontal Cortex and Frontal Pole Predict Individual Differences in Decision Impulsivity». *Brain Imaging and Behavior* 15 (1): 421–29. https://doi.org/10.1007/s11682-020-00270-1.

McIntosh, A.R., F.L. Bookstein, J.V. Haxby, e C.L. Grady. 1996. «Spatial Pattern Analysis of Functional Brain Images Using Partial Least Squares». *NeuroImage* 3 (3): 143–57. https://doi.org/10.1006/nimg.1996.0016.

Mertz, Jerome. 2011. «Optical Sectioning Microscopy with Planar or Structured Illumination». *Nature Methods* 8 (10): 811–19. https://doi.org/10.1038/nmeth.1709.

Moaddab, Mahsa, Madelyn H. Ray, e Michael A. McDannald. 2021. «Ventral Pallidum Neurons Dynamically Signal Relative Threat». *Communications Biology* 4 (1): 43. https://doi.org/10.1038/s42003-020-01554-4.

Müllenbroich, M. Caroline, Ludovico Silvestri, Leonardo Onofri, Irene Costantini, Marcel van't Hoff, Leonardo Sacconi, Giulio Iannello, e Francesco S. Pavone. 2015. «Comprehensive Optical and Data Management Infrastructure for High-Throughput Light-Sheet Microscopy of Whole Mouse Brains». *Neurophotonics* 2 (4): 041404. https://doi.org/10.1117/1.NPh.2.4.041404.

Orsini, Caitlin A., e Stephen Maren. 2012. «Neural and Cellular Mechanisms of Fear and Extinction Memory Formation». *Neuroscience & Biobehavioral Reviews* 36 (7): 1773–1802. https://doi.org/10.1016/j.neubiorev.2011.12.014.

Pezzone, Michael A., Wen-Sen Lee, Gloria E. Hoffman, e Bruce S. Rabin. 1992. «Induction of C-Fos Immunoreactivity in the Rat Forebrain by Conditioned and Unconditioned Aversive Stimuli». *Brain Research* 597 (1): 41–50. https://doi.org/10.1016/0006-8993(92)91503-7.

Ragan, Timothy, Lolahon R Kadiri, Kannan Umadevi Venkataraju, Karsten Bahlmann, Jason Sutin, Julian Taranda, Ignacio Arganda-Carreras, Yongsoo Kim, H Sebastian Seung, e Pavel Osten. 2012. «Serial Two-Photon Tomography for Automated Ex Vivo Mouse Brain Imaging». *Nature Methods* 9 (3): 255–58. https://doi.org/10.1038/nmeth.1854.

Renier, Nicolas, Eliza L. Adams, Christoph Kirst, Zhuhao Wu, Ricardo Azevedo, Johannes Kohl, Anita E. Autry, et al. 2016. «Mapping of Brain Activity by Automated Volume Analysis of Immediate Early Genes». *Cell* 165 (7): 1789–1802. https://doi.org/10.1016/j.cell.2016.05.007.

Renier, Nicolas, Zhuhao Wu, David J. Simon, Jing Yang, Pablo Ariel, e Marc Tessier-Lavigne. 2014. «IDISCO: A Simple, Rapid Method to Immunolabel Large Tissue Samples for Volume Imaging». *Cell* 159 (4): 896–910. https://doi.org/10.1016/j.cell.2014.10.010.

Ronneberger, Olaf, Philipp Fischer, e Thomas Brox. 2015. «U-Net: Convolutional Networks for Biomedical Image Segmentation». In *Medical Image Computing and Computer-Assisted*

Intervention – MICCAI 2015, a cura di Nassir Navab, Joachim Hornegger, William M. Wells, e Alejandro F. Frangi, 9351:234–41. Lecture Notes in Computer Science. Cham: Springer International Publishing. https://doi.org/10.1007/978-3-319-24574-4_28.

Roy, Dheeraj S., Young-Gyun Park, Minyoung E. Kim, Ying Zhang, Sachie K. Ogawa, Nicholas DiNapoli, Xinyi Gu, et al. 2022. «Brain-Wide Mapping Reveals That Engrams for a Single Memory Are Distributed across Multiple Brain Regions». *Nature Communications* 13 (1): 1799. https://doi.org/10.1038/s41467-022-29384-4.

Sacchetti, Benedetto, Elisabetta Baldi, Carlo Ambrogi Lorenzini, e Corrado Bucherelli. 2002. «Cerebellar Role in Fear-Conditioning Consolidation». *Proceedings of the National Academy of Sciences* 99 (12): 8406–11. https://doi.org/10.1073/pnas.112660399.

Silva, Bianca A., Simone Astori, Allison M. Burns, Hendrik Heiser, Lukas van den Heuvel, Giulia Santoni, Maria Fernanda Martinez-Reza, Carmen Sandi, e Johannes Gräff. 2021. «A Thalamo-Amygdalar Circuit Underlying the Extinction of Remote Fear Memories». *Nature Neuroscience* 24 (7): 964–74. https://doi.org/10.1038/s41593-021-00856-y.

Silvestri, L., M. C. Müllenbroich, I. Costantini, A. P. Di Giovanna, G. Mazzamuto, A. Franceschini, D. Kutra, et al. 2021. «Universal Autofocus for Quantitative Volumetric Microscopy of Whole Mouse Brains». *Nature Methods* 18 (8): 953–58. https://doi.org/10.1038/s41592-021-01208-1.

Simerly, Richard B. 2002. «Wired for Reproduction: Organization and Development of Sexually Dimorphic Circuits in the Mammalian Forebrain». *Annual Review of Neuroscience* 25 (1): 507–36. https://doi.org/10.1146/annurev.neuro.25.112701.142745.

Smith, Kara M., e Nabila Dahodwala. 2014. «Sex Differences in Parkinson's Disease and Other Movement Disorders». *Experimental Neurology* 259 (settembre): 44–56. https://doi.org/10.1016/j.expneurol.2014.03.010.

Susaki, Etsuo A., Kazuki Tainaka, Dimitri Perrin, Fumiaki Kishino, Takehiro Tawara, Tomonobu M. Watanabe, Chihiro Yokoyama, et al. 2014. «Whole-Brain Imaging with Single-Cell Resolution Using Chemical Cocktails and Computational Analysis». *Cell* 157 (3): 726–39. https://doi.org/10.1016/j.cell.2014.03.042.

Tonegawa, Susumu, Mark D. Morrissey, e Takashi Kitamura. 2018. «The Role of Engram Cells in the Systems Consolidation of Memory». *Nature Reviews Neuroscience* 19 (8): 485–98. https://doi.org/10.1038/s41583-018-0031-2.

Vetere, Gisella, Justin W. Kenney, Lina M. Tran, Frances Xia, Patrick E. Steadman, John Parkinson, Sheena A. Josselyn, e Paul W. Frankland. 2017. «Chemogenetic Interrogation of a Brain-Wide Fear Memory Network in Mice». *Neuron* 94 (2): 363-374.e4. https://doi.org/10.1016/j.neuron.2017.03.037.

Werling, Donna M., e Daniel H. Geschwind. 2013. «Sex Differences in Autism Spectrum Disorders»: *Current Opinion in Neurology* 26 (2): 146–53. https://doi.org/10.1097/WCO.0b013e32835ee548.

Wheeler, Anne L., Cátia M. Teixeira, Afra H. Wang, Xuejian Xiong, Natasa Kovacevic, Jason P. Lerch, Anthony R. McIntosh, John Parkinson, e Paul W. Frankland. 2013. «Identification of a Functional Connectome for Long-Term Fear Memory in Mice». A cura di Olaf Sporns. *PLoS Computational Biology* 9 (1): e1002853. https://doi.org/10.1371/journal.pcbi.1002853.

Wu, Zheng, Ashok Litwin-Kumar, Philip Shamash, Alexei Taylor, Richard Axel, e Michael N. Shadlen. 2020. «Context-Dependent Decision Making in a Premotor Circuit». *Neuron* 106 (2): 316-328.e6. https://doi.org/10.1016/j.neuron.2020.01.034.

Yang, Cindy F., e Nirao M. Shah. 2014. «Representing Sex in the Brain, One Module at a Time». *Neuron* 82 (2): 261–78. https://doi.org/10.1016/j.neuron.2014.03.029.

Zucker, Irving, e Annaliese K. Beery. 2010. «Males Still Dominate Animal Studies». *Nature* 465 (7299): 690–690. https://doi.org/10.1038/465690a.